Maximising Branch Power Flows as a Descriptive Structural Metric for Electrical Networks

Paul Cuffe, *Member, IEEE*

***Abstract*—This paper describes an optimization-based procedure that identifies the maximum power flow that each branch in an electrical network could be exposed to. The procedure uses a linear optimal power flow formulation that determines the flow-maximising generator dispatch and loading conditions for each branch in turn. This theoretical upper bound on the power flow that a branch could be exposed to is termed its *loadability*. The paper proposes this loadability as a descriptive structural metric that helps reveal the fundamental origin of congestion in power system. For instance, it is insightful to compare a branch's loadability with its as-built thermal capacity, to identify those branches that are most congestion-prone, or alternatively, those lines which can never exploit their full available capacity. In the six test systems studied, it is found that there is wide variation in the loadability of the various branches, where some would be loaded well beyond their thermal limits by particular generating schedules, whereas other branches can never operate beyond even a fraction of their thermal capabilities. Low branch reactance is found to be a key driver of high loadability in power systems, and this suggests new approches to alleviating transmission system congestion.**

I. Introduction

A. Motivation

THIS paper proposes an optimization procedure to quantify the *maximum possible* power flow that each branch in an electrical network could be exposed to. Power lines are assets of national importance which are constructed at considerable expense [1], [2]. A line's thermal rating is an important parameter to consider when a branch is being added to a network [3], as this ampacity is often the binding constraint on how much power it can transmit (though longer lines, and those at very high voltages, may more typically be constrained by voltage stability limits [4], [5])

If thermal limits are too low, the system may regularly experience *congestion*, whereby the desired generation schedules cannot be accommodated, and more expensive alternative generation sources have to be used instead [6]. On the other hand, specifying overly-generous thermal limits may increase the capital cost of grid construction for little benefit [7]. The core motivation of the present work is to explore how this trade-off [8] has been handled in some well-known test systems, and thereby to point towards the *fundamental causes* of transmission system congestion. The novel optimization-based screening procedure permits exploration of power system congestion in a general sense, by identifying the subset of branches which are at least theoretically capable of being loaded beyond their thermal limits. Identifying the congestion-prone branches within a system should offer actionable insights for identifying and validating remedial measures, such as strategically removing [9], [10] or increasing the reactance [11]–[13] of particular lines to better balance power flows, or selectively uprating [14]–[16] particular branches. Other potential applications for the procedure are prioritising maintenance planning [17] and identifying anomalous lines (those with unusually high or low loabability) for further investigation.

P. Cuffe (paul.cuffe@ucd.ie) is with the School of Electrical and Electronic Engineering, University College Dublin. This work has emanated from research conducted with the financial support of Science Foundation Ireland under the SFI Strategic Partnership Programme Grant Number SFI/15/SPP/E3125. The opinions, findings and conclusions or recommendations expressed in this material are those of the author and do not necessarily reflect the views of the SFI.

B. Literature review

While optimal power flow techniques have been applied to a broad range of problems over their long history [18], [19], the author is not aware of any works that have explicitly characterised the maximum active power flow each branch might be exposed to (notwithstanding [20], a precursor to the present manuscript)

The proposed optimization procedure takes inspiration from [21], which used linear programming to calculate the absolute maximum load that could feasibly be met by a combined generation/transmission system. Other works applying optimisation techniques to characterise the extremal operating envelopes of power system components include [22], [23], which used capability charts to describe feasible complex power combinations for, respectively, grid operational configurations and wind energy harvesting networks.

Work in [24] proposed a maximum-flow based approach to identify vulnerable lines in a power system. Their technique considered power exchanges between each source and sink pair in the network digraph, and defined a new centrality metric based on each branch's participation in these notional transactions. This technique could be viewed as adapting the idea of *betweeness centrality* [25], [26] to the electrical context. The authors of [24] validated the applicability of their new centrality metric by showing that the failures of the lines they identified as vulnerable were more damaging to the network.

Work in [27] extended the maximum-flow approach of [24] by including a vertex weighting procedure. Again, the proposed

use case of the metric in [27] is in ranking branches for vulnerability assessment. Other works proposing line centrality measures for vulnerability screening include [28], [29]. More generally, numerous algorithms exist which attempt to gauge the importance of a node or edge in a generic complex network [30], [31], and various authors have adapted these for electrical grids [32]–[35].

On the other hand, work in [36] simulated branch interdiction attacks on a number of power systems in many operational states, and this broad-based analysis did not find that the trialled topological vulnerability measures were a particularly effective way to choose branch attack targets. Such a finding is consistent with work in [37].

Beyond the vulnerability analysis application area, work in [38] proposed a line centrality measure to describe the role of each branch in facilitating circulating and load-serving current flows in an electrical network, under the paradigm of [39]. Work in [40] examined that maximum power flow that a particular line may be exposed to under certain contingency situations, and used this characterisation within a transmission cost allocation scheme.

C. Contribution and paper organisation

The core contribution of the present paper is articulating a novel procedure that reveals the maximum line flows that each branch in a power system may be required to carry. Those branches with unusually high loadability may be seen as critical or central lines in the system, which may be especially important in terms of causing congestion, or may be prioritised for maintenance planning [17]. Conversely, branches with unusually low loadability may be identified as partially obsolete or marginalised assets.

By comparing loadability with available thermal capacity, the most congestion-prone branches within a power system can be directly identified, and these may be apt candidates for uprating [14]–[16] or for the addition of static or controllable reactance [11]–[13].

Finally, the novel loadability metric can offer scientific insights into the structure and function of power transmission networks [41]. While abstract topological metrics may only offer limited insights into transmission network operation (see [36], [37], [42]–[44] for various skeptical perspectives), the proposed metric has a tangible interpretation rooted in the the actual dynamics of physical power flow. Importantly, this allows the costly phenomenom of power system congestion [6], [8] to be analysed in a general and fundamental way. The present manuscript emphasises this aspect, and uses a data-driven approach to explore the determinants of branch loadability and congestion in several test power systems.

The paper is organized as follows: Section II describes the optimal power flow procedure for calculating branch loadability. The test platform is described in Section III, and Section IV provides several perspectives on the calculated loadability dataset, to elucidate the structural origins of power system congestion, which then informs the conclusions in Section V.

II. Methodology

A. Calculating maximum branch power flows

A linear programme is sequentially invoked for every branch b in a network, to maximise the power flow $\boldsymbol{f}$ it carries. This optimization is calculated for both flow directions on the branch, one after the other. The first objective function for a branch b connecting buses i and j is:

$$\boldsymbol{f}^*_{b|i\rightarrow j} = max(\boldsymbol{f}_{b|i\rightarrow j}) \tag{1}$$

And then likewise for the direction $j \rightarrow i$.

Decision variables in this optimization include the power output $\boldsymbol{p}$ for each generator, g. Each generator's online status ($\boldsymbol{s}$, binary) is incorporated alongside its minimum and maximum operating limit parameters, P^+_g and P^-_g as follows:

$$\boldsymbol{s}_g P^-_g \leq \boldsymbol{p}_g \leq \boldsymbol{s}_g P^+_g \tag{2}$$

Generator costs parameters are not relevant to this formulation, as a *characterisation* of the worst-case power injection profile is being sought, without consideration of the cost or likelihood of the schedule that would cause this (see [23]) Leaving the generation scheduling free in this way also models the effects of generator contingencies. In other contexts, it may be desirable to model generator costs and correlations between renewable generator outputs: a simple formulation is chosen here to give the worst case loadabilities and to maintain clarity in this first exposition of the procedure.

To find the system-wide demand conditions that permit a branch's maximum loading, nodal spot demands are scaled uniformly relative to their parametrised maxima P^+_d:

$$\boldsymbol{p}_d = k.P^+_d \tag{3}$$

This scalar demand level k remains a free variable in the optimization, bound between some limits $K^- \leq k \leq K^+$ (this uniform load scaling approach has been assumed for simplicity, but it would also reasonable to control spot loads individually or zonally to identify the flow-maximising conditions)

A power balance is enforced at every bus, where the vector $\boldsymbol{p}_{d|n}$ describes the sum of power demands and $\boldsymbol{p}_{g|n}$ the sum of generation at each node n. The nodal balance also includes the vector of branch power flow, $\boldsymbol{f}_b$, and the system's incidence matrix, $A_{(b\times n)}$:

$$\boldsymbol{p}_{g|n} + \boldsymbol{p}_{d|n} = \boldsymbol{f_b}^T A \tag{4}$$

For a branch connecting bus i to bus j, with reactance X_b, the power flow is determined by the voltage angle, $\boldsymbol{\phi}$, difference that prevails. Logical constraints are included to allow the line removal decisions that model contingencies, using the vector of binary decision variables $\boldsymbol{o}_b$:

$$\boldsymbol{f}_{b|i\to j} = \begin{cases} \frac{\boldsymbol{\phi}_i - \boldsymbol{\phi}_j}{X_b} & \forall\ \boldsymbol{o}_b = 0 \\ 0 & \forall\ \boldsymbol{o}_b = 1 \end{cases} \tag{5}$$

The number of branch outages contingencies to be considered is imposed by summing the vector of binary variables and comparing with the cardinality of the branch set, $card(B)$:

$$\sum_b \boldsymbol{o}_b \geq card(B) - C \tag{6}$$

So for instance, setting $C = 2$ would find maximum branch loadings under $(N-2)$ conditions i.e permitting the optimization to remove two other lines when maximising the flow in a particular branch.

Branch thermal limits are not enforced, as the *maximum* conceivable flows that a dispatch profile could invoke is the metric of interest, regardless of whether this would overload the line in question, or indeed may overload lines elsewhere in the network. This is modelling decision specific to the present manuscript: it may also be useful and insightful to impose thermal limits on every other branch *except* the branch whose flow is being maximised, as this will identify situations where other branchs' thermal capacities impede a particular branch's theoretical maximum flow. Instead, the present decision to disregard thermal limits explores how a branch's reactance, and its position with the network structure, affects its maximum flow levels.

The optimal power flow problem can be formulated at various levels of model accuracy, and the present exposition uses a simple linear dc formulation. This simplification means that voltage magnitude, reactive power flows and the impact of sophisticated control schemes [45] are not modelled. This simple analysis was chosen to directly showcase the fundamental drivers of branch loadability and congestion; the grid's connective structure and the reactance of different lines. The same branch flow maximisation approach could readily be implementing using more realistic ac optimal power flow formulations [46], [47]. Notably, reactive power flows tend to increase the current loading of ac power lines, so a formulation including these would tend to identify higher line loadabilities.

B. Branch structural metrics

1) Loadability definition: When the two optimization calculations have been performed for all branches in the power system, the $\boldsymbol{f}^*$ vectors will be fully populated. To extract useful information from these, we define the concept of branch *loadability*. This metric, $\boldsymbol{l}_b$, has units of MW and records the absolute maximum power flow that could arise on each branch. It is calculated by taking the absolute values $|\boldsymbol{f}^*_{b|i\to j}|$ and $|\boldsymbol{f}^*_{b|j\to i}|$ and selecting the greater:

$$\boldsymbol{l}_b = \begin{cases} |\boldsymbol{f}^*_{b,i\to j}| & \forall\ |\boldsymbol{f}^*_{b,i\to j}| > |\boldsymbol{f}^*_{b,j\to i}| \\ |\boldsymbol{f}^*_{b,j\to i}| & \forall\ |\boldsymbol{f}^*_{b,j\to i}| > |\boldsymbol{f}^*_{b,i\to j}| \end{cases} \tag{7}$$

TABLE I
TEST SYSTEM CHARACTERISTICS

	#Bus	#Branch	#Gen	∑Load	∑Gen
ln_nesta_case73_ieee_rts	73	120	99	8.9 GW	10.2 GW
ln_nesta_case118_ieee	118	186	54	6.2 GW	7.1 GW
ln_nesta_case189_edin	189	206	35	2.6 GW	3.0 GW
ln_nesta_case162_ieee_dtc	162	284	12	8.4 GW	9.7 GW
ln_nesta_case1460wp_eir	1460	1924	285	9.3 GW	10.7 GW
ln_nesta_case2224_edin	2224	3207	394	97.2 GW	111.8 GW

By comparing against the rated thermal capacity parameter for a branch, F^+_b, we can also define the *loadability ratio*, which describes the proportional loading of the branch in the worst-case conditions:

$$\boldsymbol{r}_b = \frac{\boldsymbol{l}_b}{F^+_b} \tag{8}$$

2) Branch radiality index: Branch loadability may be related with how well meshed the particular line is within the network. That is, does a particular line have many other lines in parallel with it, or is it a standalone radial branch? To allow this to be explored rigorously, this section defines a static structural metric, *branch radiality index*, for each branch: $\mathfrak{R}_b$. This new metric is extracted from the *Power Transfer Distribution Factors* [48] for the system. A vector $\Phi_{b|k\to l}$ can be constructed that records the incremental active power loading on all branches b in the system, considering a 1 MW power injection at an arbitrary bus k and withdrawal at bus l. To determine the branch radiality index $\mathfrak{R}_{b|i\to j}$, the $\Phi_{b|k\to l}$ vector is constructed for each branch in turn, setting $k = i$ and $l = j$, where i is the sending bus and j the receiving bus for that particular branch. Therefore, for each branch we calculate an incremental 1 MW power transaction injected at that branch's sending bus and withdrawn at its receiving bus. Extracting $\mathfrak{R}_{b|i\to j}$ from the corresponding element of $\Phi_{b|k\to l}$ identifies what portion of this transaction the branch itself carries. For a purely radial branch, with no redundant parallel paths, the full 1 MW would flow along the branch itself; conversely, where an abundance of lower reactance parallel paths are available, only a small fraction of the 1 MW transaction will flow on the branch itself. Therefore:

$$0 \leq \mathfrak{R}_b \leq 1 \tag{9}$$

This notion of branch radiality index is reminiscent of the concept of *shortcut edges* [49] for graph geodesics.

III. Test Platform

Simulations are performed in MATLAB using MATPOWER [50], YALMIP [51] and GUROBI [52]. Six test systems are considered, taken from [53]. These systems were chosen as they are well-known and widely used, and span across small, medium and large networks. To ensure that these could be compared fairly,

TABLE II
DESCRIPTIVE STATISTICS

	Loadability (MW)				Loadability Ratio (pu)			
	Min	Median	Max	Skewness	Min	Median	Max	Skewness
ln_nesta_case73_ieee_rts	51.55	271.79	1155.09	1.58	0.27	0.73	2.31	1.47
ln_nesta_case118_ieee	1.66	91.90	1106.68	2.94	0.01	0.56	3.19	1.79
ln_nesta_case189_edin	0.00	38.39	402.22	1.67	0.00	0.22	2.50	2.22
ln_nesta_case162_ieee_dtc	2.23	80.39	1282.01	2.71	0.05	0.56	2.42	1.30
ln_nesta_case1460wp_eir	0.00	22.87	799.56	3.81	0.00	0.26	2.15	1.32
ln_nesta_case2224_edin	0.00	110.85	6146.01	3.17	0.00	0.47	7.86	2.63

their aggregate maximum demand levels were normalised so that operating at $k = 1$ leaves an available generation reserve margin equal to 15% of installed capacity, a limit consistent with [54]. K^+ was set = 1 and $K^- = 0.25$

The system names are prepended with 'ln' to denote this load normalisation. Details of these normalised systems are provided in Table I. The raw data and calculation scripts underlying the results are available in a persistent online repository at [55].

IV. RESULTS

A. Intact system conditions

Initially, C was set = 0 to model intact $(N - 0)$ conditions.

1) Branch loadability trends: Descriptive statistics describing the loadability, $\boldsymbol{l}_b$, and loadability ratio, $\boldsymbol{r}_b$, of the branches in each system are provided in Table II. One fact is immediately apparent: the median loadability ratio is below unity in every case. This means that the median branch in each system cannot be loaded beyond its thermal limits in even the most onerous dispatch and aggregate demand conditions. Furthermore, on five of the six test systems, the minimum loadability is zero or negligible. Median loadability is quite low, while max loadability is quite high, and all of these distributions exhibit a rightward skew. Histograms showing these distributions explicitly for loadability ratio are provided in Fig. 1. The diversity in system performance is quite notable, with loadability ratios above unity barely represented in 'case1460wp_eir', although relatively common on 'case2224_edin'.

To explore these trends further, the relationship between branch loadability, $\boldsymbol{l}_b$, and branch thermal rating, F_b^+, is shown as a matrix of scatterplots in Fig. 2. Logarithmic scales are used for each axis. The points are coloured based on binning each branch into one of five categories as below:

Loadability < 2 MW	$\Longrightarrow$	**Negligible**
Loadability ratio < 0.5	$\Longrightarrow$	**Light**
0.5 < Loadability ratio < 1	$\Longrightarrow$	**Moderate**
1 < Loadability ratio < 2	$\Longrightarrow$	**Overloadable**
2 < Loadability ratio	$\Longrightarrow$	**Severe**

These colour encodings are used throughout this manuscript to denote these branch categories. The preponderance of greens and greys in Fig. 2 indicates that most branches in these intact systems can never experience thermal congestion, and this is also shown explicitly in Fig. 4. For all six test sytems, less than 20% of branches can ever be overloaded, even in worst-case demand and dispatch conditions.

Considering the marginal distributions to the right of the panes in Fig. 2, it is evident that for three of the systems ('case189_edin', 'case1460wp_eir' and 'case2224_edin'), there is a prominent and discontinuous peak at the bin representing 0 to 1 MW of loadability, implying that these systems contain many branches that can never carry significant power. This is a surprising result that invites questions about how these test systems were constructed (see [56]). These histograms otherwise appear to follow an approximate bell shape on their logarithmic scales, perhaps suggesting an underlying lognormal type distribution (The frequency distributions of loadability and loadability ratio are also shown, inter alia, in Fig. 9 and 10.)

Distribution fitting using three parametric distributions of this general type was applied to the loadability data (exclusive of the **negligible** branches), and the results are shown in Table III. While none of these parametric distributions describes all the test systems, overall Table III supports a conclusion that branch loadability should be thought of as a long-tailed type of phenomenon.

2) Aggregate system demand levels: It might be expected that maximising a branch's loading would require high demands levels across a system. This is not so, however, as shown in Fig. 3. These histograms show the distribution of aggregate system demand levels, k, that were found to optimally maximise loadability for each branch i.e $argmax(\boldsymbol{l}_b)$. In many cases, low or intermediate system demand levels were found to facilitate the most congesting dispatches. The distributions of k appear multi-modal and discontinuous, and these histograms do not point towards any particular parametric distribution.

3) Loadability and network structure: To depict the relationship between system structure, branch location, and loadability category, network diagrams of the six test systems are provided in Fig. 5. These diagrams are drawn using the technique in [57], which positions nodes using a measure of electrical distance. For most of the systems, it appears that the high loadability branches are located in the meshed core of the system. Branches in the sub-transmission and distribution networks cannot typically be loaded beyond their thermal limits.

To further explore the role of branch messhing, the relationship between branch radiality index $\mathfrak{R}_b$ and loadability $\boldsymbol{l}_b$ is

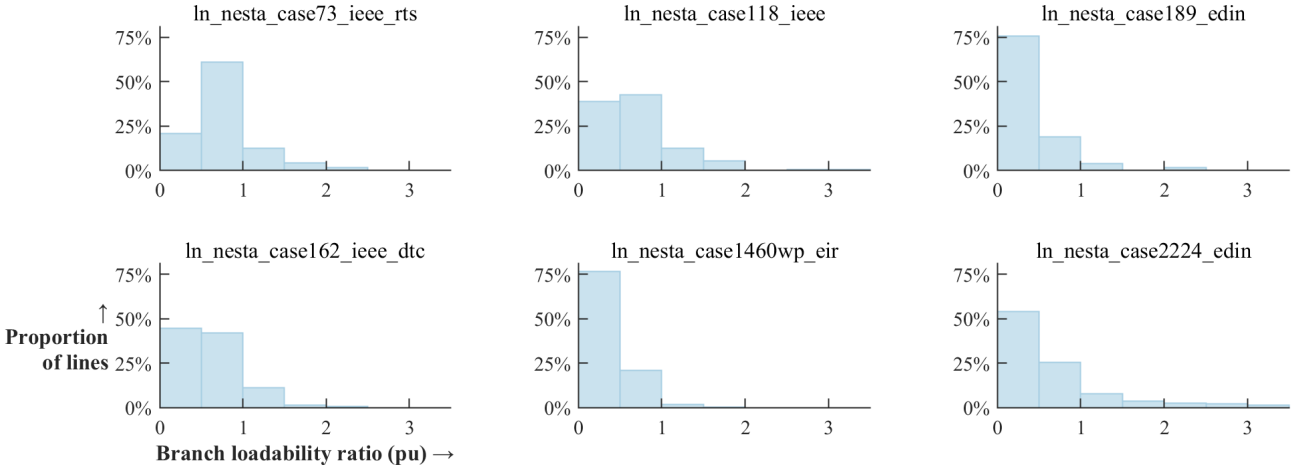

Fig. 1. Histograms showing the the distribution of branch loadability ratio for each system

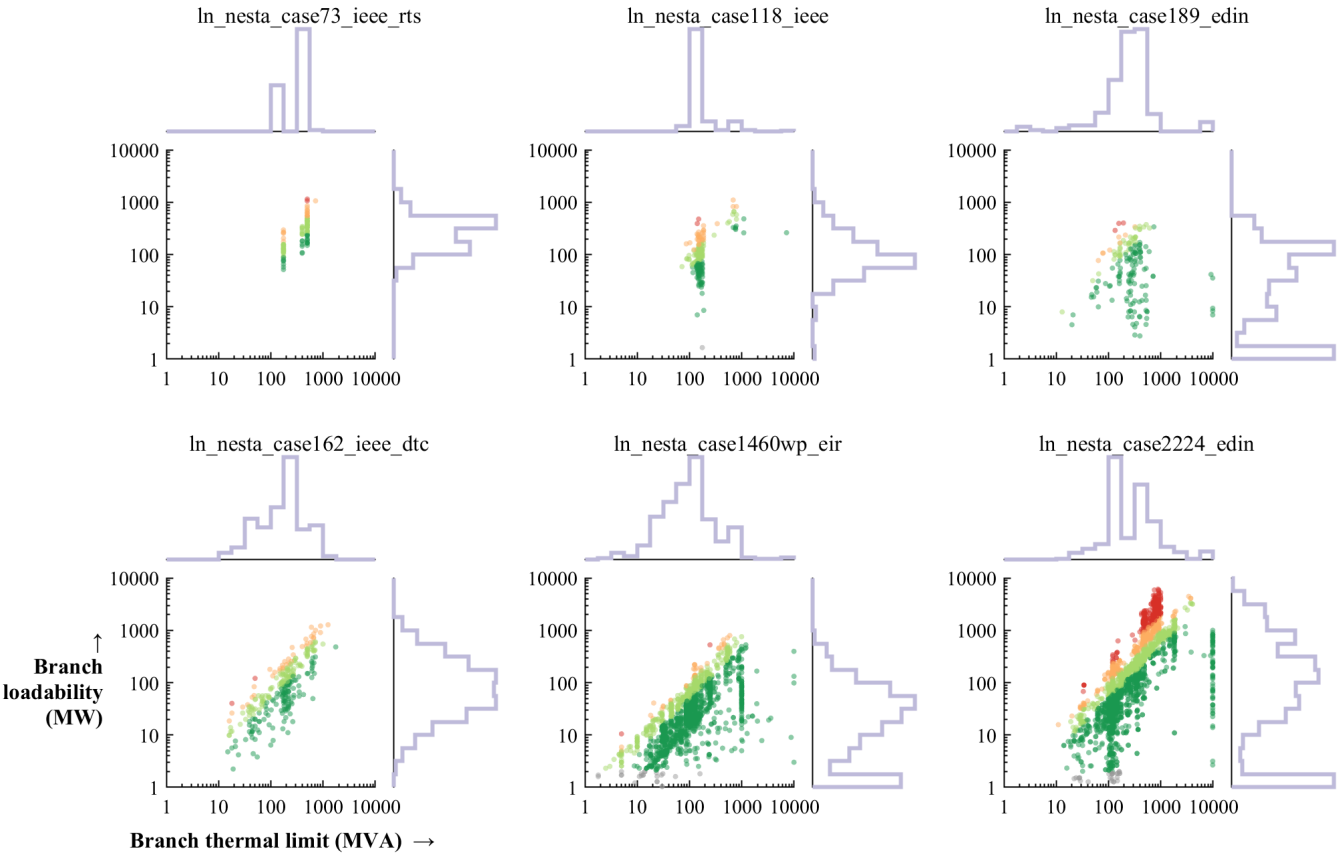

Fig. 2. Scatterplots of loadability versus branch thermal limits, shown on log-log scales with marginal distributions

TABLE III
DISTRIBUTION FITTING AND GOODNESS-OF-FIT TESTING FOR LOADABILITY

	Lognormal			Gamma			GeneralizedPareto			
	χ^2 test p	μ	σ	χ^2 test p	a	b	χ^2 test p	k	σ	θ
ln_nesta_case73_ieee_rts	0.101	5.534	0.665	0.300	2.534	123.289	*0.026	-0.285	393.952	0
ln_nesta_case118_ieee	0.304	4.605	0.845	*0.002	1.465	99.664	0.302	0.051	138.480	0
ln_nesta_case189_edin	*0.002	3.921	1.232	0.111	0.971	94.432	0.097	-0.005	92.115	0
ln_nesta_case162_ieee_dtc	0.066	4.351	1.236	*0.003	0.851	182.073	0.098	0.302	109.935	0
ln_nesta_case1460wp_eir	*p <0.001	3.399	1.202	*p <0.001	0.835	72.653	*p <0.001	0.338	40.381	0
ln_nesta_case2224_edin	*p <0.001	5.008	1.642	*p <0.001	0.540	885.041	*p <0.001	0.842	164.017	0

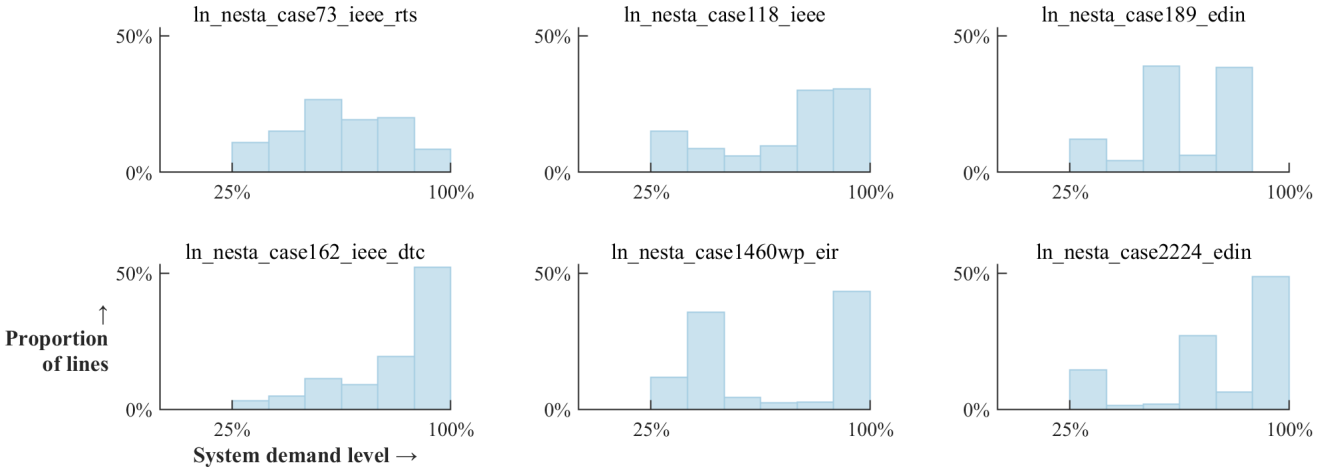

Fig. 3. The distribution of aggregate demand level that achieved the maximum loadability for each branch

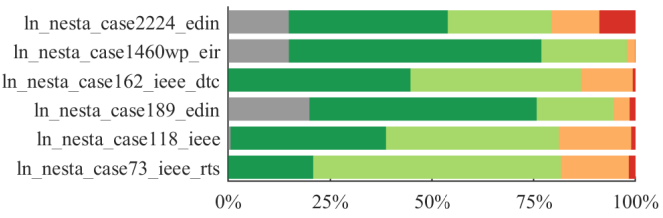

Fig. 4. Branch category histograms for each test system: only the orange and red segments to the right denote branches that can be overloaded

explored in Fig. 6. It can be noted that there is a preponderance of points at the rightmost edge of each pane, corresponding to fully radial branches. In particular, 'case189_edin' is composed mostly of these radial branches. However, the totality of Fig. 6 indicates that the full range of loadability values is possible for radial branches. Furthermore, there is no obvious relationship between the branch radiality index and loadability levels, as each category of branch loadability is represented across the full range of radiality index.

The relationship between branch reactance X_b and loadability $\boldsymbol{l}_b$ is explored in Fig. 7, which uses log-log scales. Intuitively, a branch with lower reactance would be anticipated to typically carry more power than a higher reactance branch. For all six systems, a similar envelope is formed, whereby the highest loadability arises for the lowest reactance lines. The linearity of the upper boundary of this envelope is striking and is most clearly shown for the three systems depicted in the bottom row. These envelopes in Fig. 7 may indicate that congestion arises in transmission systems where branches have overly-low levels of reactance without appropriately high thermal ratings. This might suggest that artificially adding fixed reactances to congestion-prone lines may be a viable mitigation strategy, at least in some cases.

To further explore such structural determinants, Fig. 8 relates each branch's loadability $\boldsymbol{l}_b$ to its *operating voltage*, defined as the average of the nominal voltage at its sending and receiving buses i and j (i.e transformer branches will take on an intermediate value) The trends in Fig. 8 correspond with Fig. 5: branch loadabilities typically rise steeply when ascending through the voltage levels (again, note carefully the logarithmic vertical axis) This indicates that the most heavily loadable and congestion-prone lines are found in the high voltage core of a network.

B. Loadability considering branch removals

This section provides a comparative analysis, presenting loadability and ratio figures for degraded system conditions. Due to the computational complexity of these calculations, they have only been performed for the three smaller test systems.

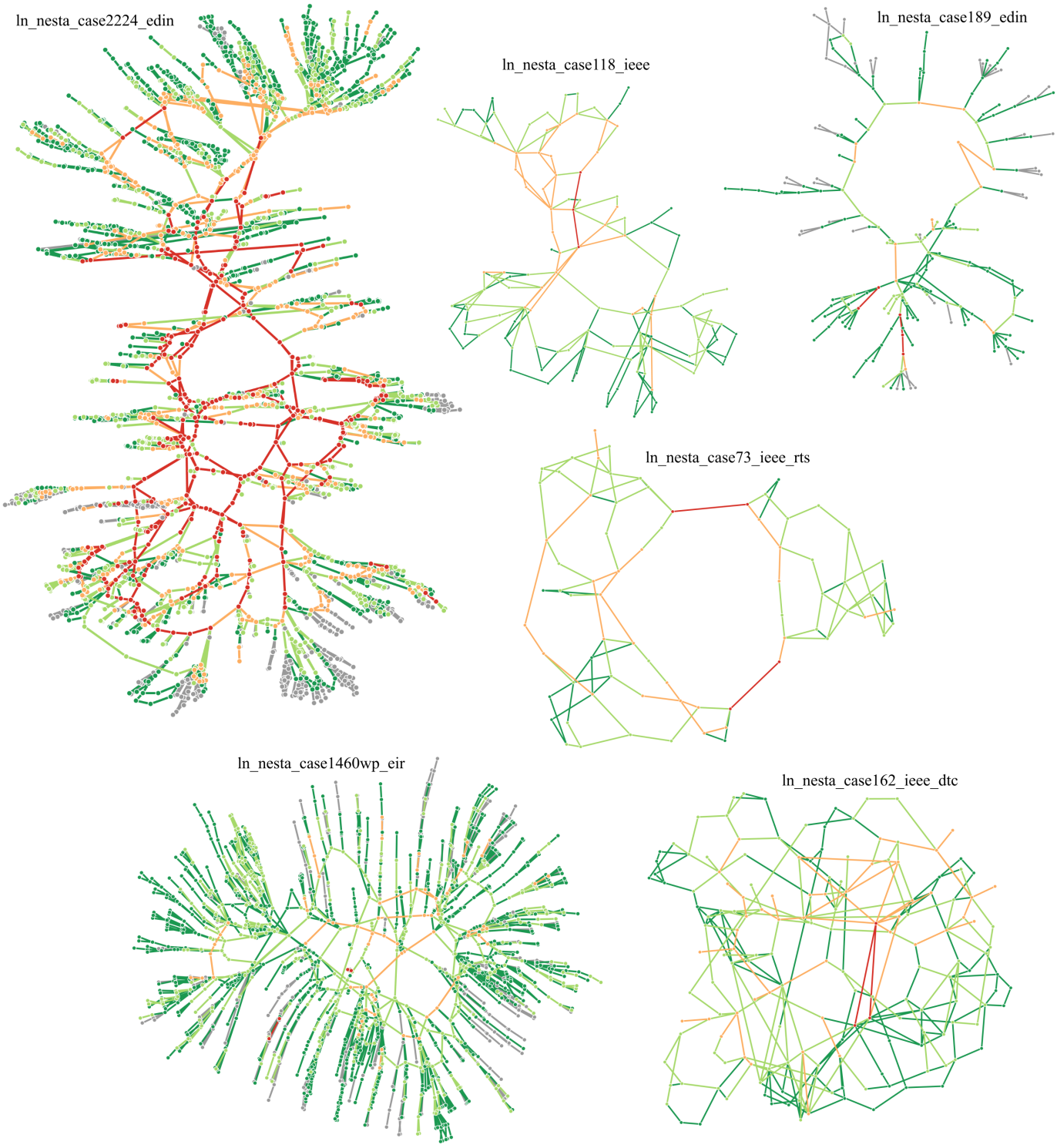

Fig. 5. Diagrams of each test system, with branches coloured according to their loadability classification

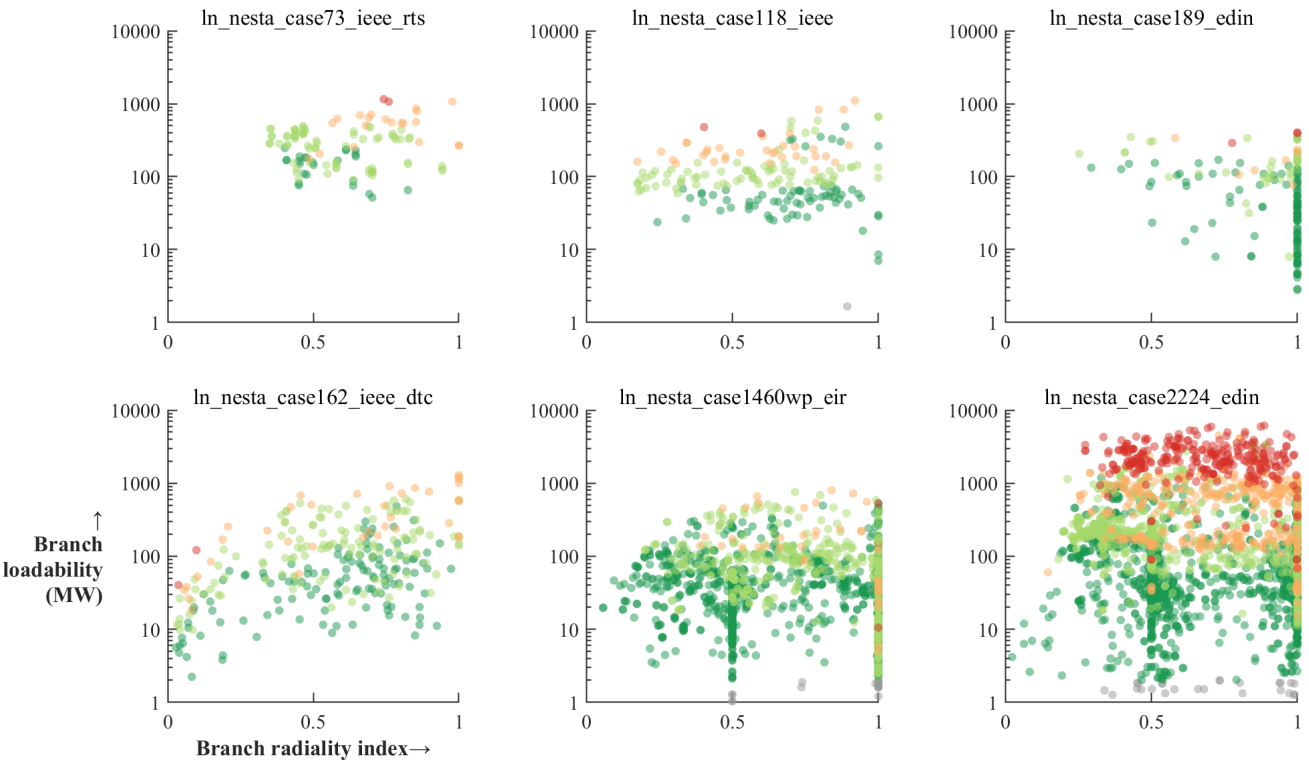

Fig. 6. The relationship between branch radiality index and loadability, shown on a log vertical scale

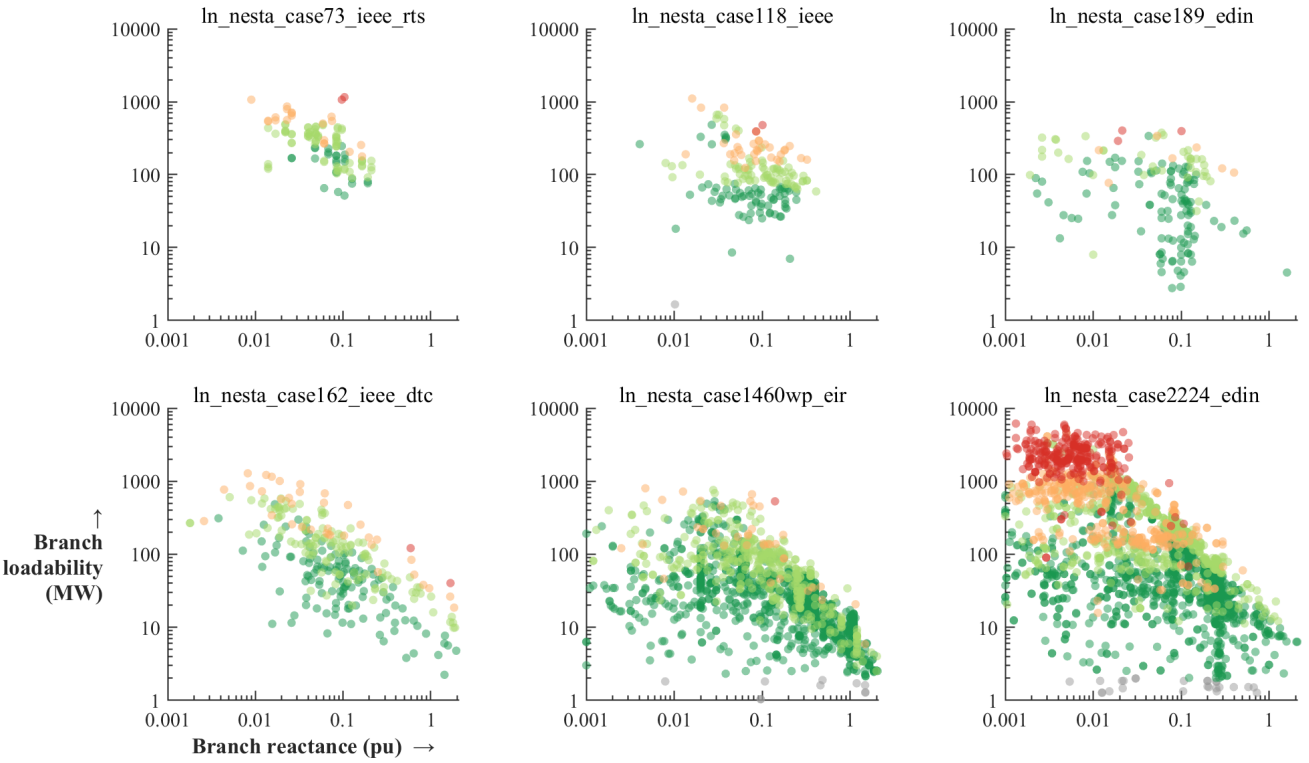

Fig. 7. The relationship between branch reactance and loadability, shown on log-log scales

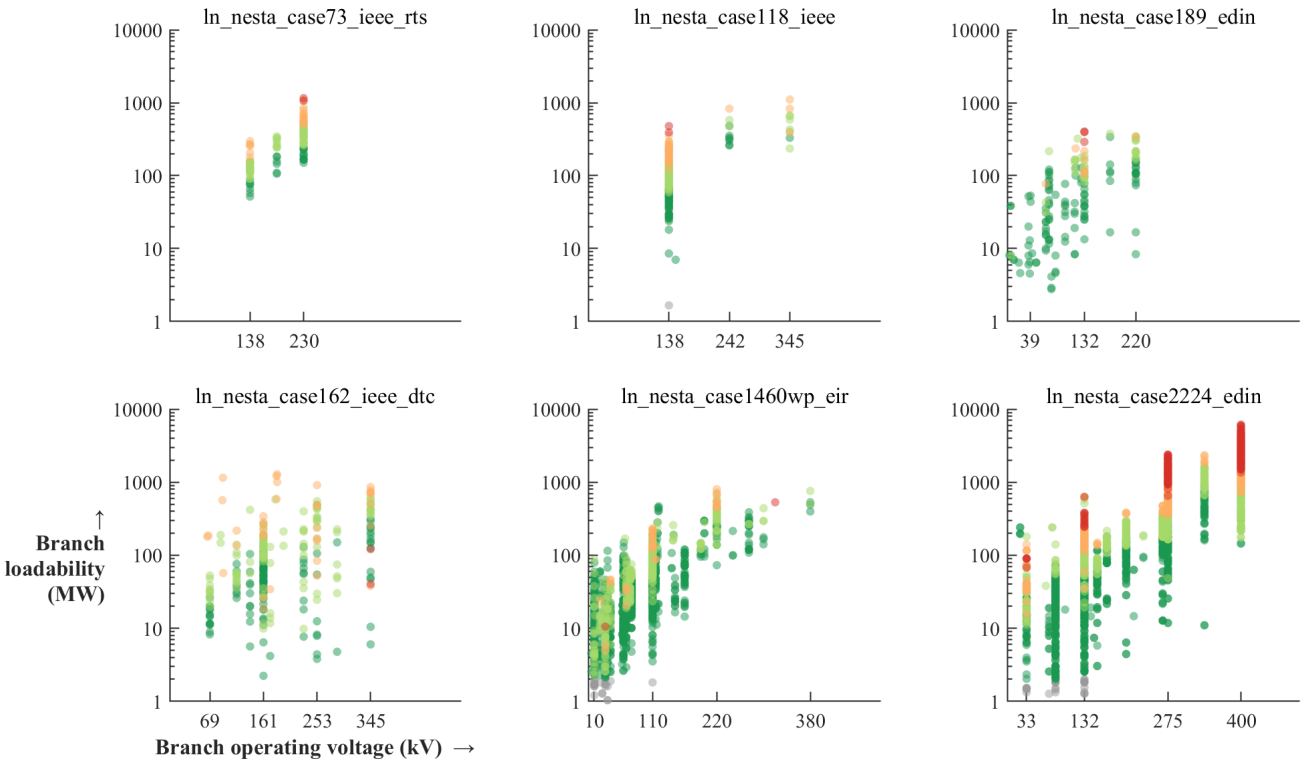

Fig. 8. The relationship between branch operating voltage and loadability, shown on a log vertical scale

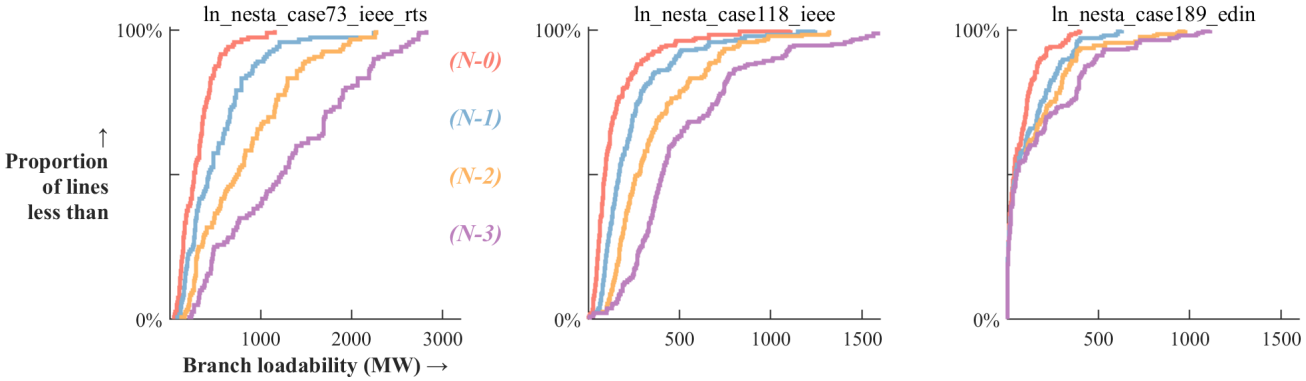

Fig. 9. The empirical cumulative distribution of branch loadability, show for various levels of branch removal contingency

As can be seen in the empirical cumulative distribution functions in Fig. 9, there is a progressive increase in branch loadabilities as system conditions degrade towards $(N-3)$. This is reflected in Table IV, which shows that median loadability increases sharply as more outages are considered. Notably, 'case189_edin' appears less vulnerable to these contingencies, as it exhibits a less marked increase in branch loadability.

A similar effect is also shown in Fig. 10, which shows the loadability ratios on a linear horizontal axis. It can be seen that the portion of lines with a loadability ratio above unity grows as more outages are considered, with the majority of branches becoming overloadable in $(N-2)$ or $(N-3)$ conditions. This is shown explicitly in Fig. 11, which shows a clear increase in the number of **overloadable** and **severe** branches as contingency conditions deepen. On the other hand, the totality of Fig. 11 shows a notable diversity in branch loadability categorisations across the spectrum of contingency conditions, with **severe** branches present in intact networks, and **light** branches in networks enduring $(N-3)$ conditions.

However, considering Table V shows that even under $(N-1)$ degraded conditions, the median loadability ratio is near or below unity for these three test systems. It appears that 'case118_edin' is somewhat more resilient against outage-induced overloading compared to 'case73_ieee_rts'.

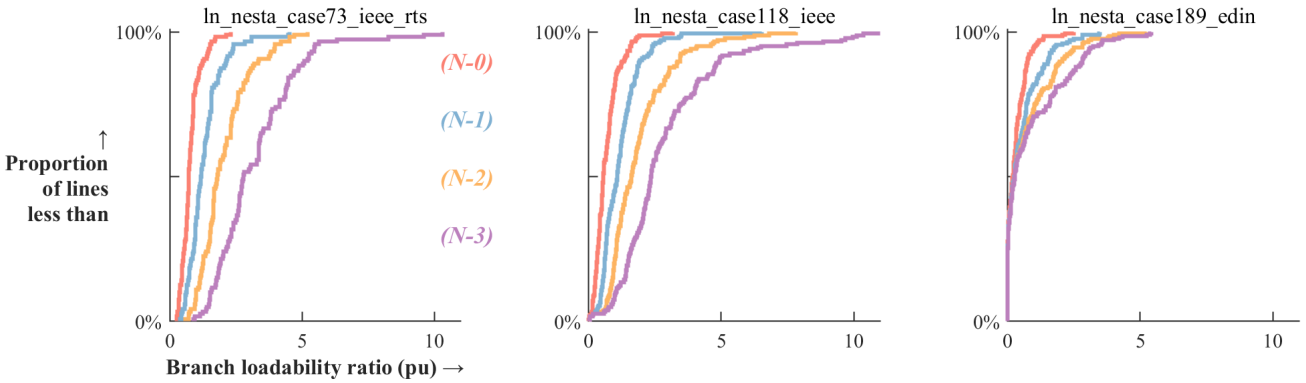

Fig. 10. The empirical cumulative distribution of branch loadability ratio, show for various levels of branch removal contingency

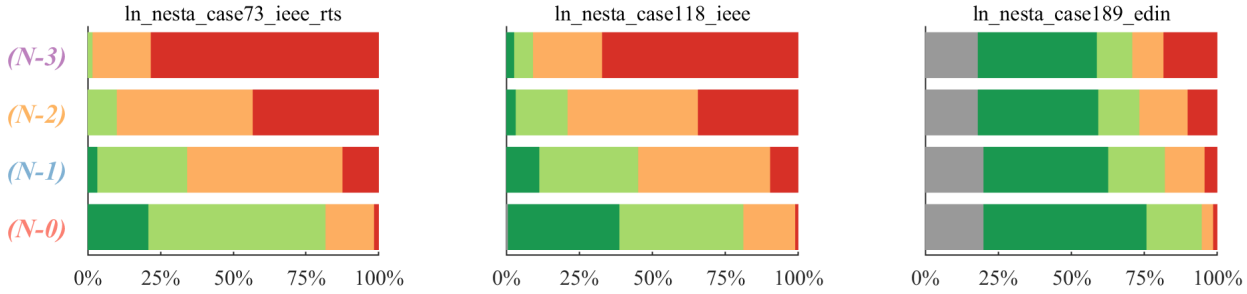

Fig. 11. Branch categorisation proportion shown by colour, for each system at each level of contingency

TABLE IV
MEDIAN LOADABILITY IN DEGRADED CONDITIONS (MW)

	(N - 0)	*(N - 1)*	*(N - 2)*	*(N - 3)*
ln_nesta_case73_ieee_rts	271.8	433.8	751.0	1232.0
ln_nesta_case118_ieee	91.9	169.4	273.9	404.9
ln_nesta_case189_edin	38.4	46.0	51.9	51.9

TABLE V
MEDIAN LOADABILITY RATIO IN DEGRADED CONDITIONS (PU)

	(N - 0)	*(N - 1)*	*(N - 2)*	*(N - 3)*
ln_nesta_case73_ieee_rts	0.73	1.18	1.79	2.79
ln_nesta_case118_ieee	0.56	1.09	1.63	2.36
ln_nesta_case189_edin	0.22	0.28	0.28	0.28

Interesting, the loadability ratio for ‘case189_edin’ does not shift right as markedly as more line outages are considered: this is likely because of the preponderance of radial lines in this system. As these branches are not meshed, their power flow is entirely determined by the downstream demand or upstream generator they serve, and so cannot be affected by removing other lines.

V. DISCUSSION

Several key findings have emerged from the analysis of branch loadability in the six test systems:

- The loadability for many branches was found to be near-zero, which may suggest anonomalies in how these test systems were constructed [56].
- Branch loadability appeared to follow an approximately lognormal distribution, showing this to be a long-tailed type of phenomenon. Most branches cannot be heavily loaded, but a few can be loaded to extreme levels.
- Branch reactance appeared to be a key driver of loadability, with the most heavily overloadable lines generally having the lowest reactance. A linear envelope was evident on the log-log plots of these quantities. This relationship highlights that a branch’s thermal rating should be commensurate with its reactance if congestion is to be avoided. Devices are available to statically or dynamically modulate a branch’s impedance [58].
- When degraded system conditions were considered by permitting branch removals, loadabilities increased markedly, although remaining quite widely distributed.

VI. CONCLUSIONS

This paper deployed an optimisation procedure to determine the maximum power flow each branch in an electrical network

could be exposed to. On the six test systems considered, it was found that, under intact network conditions, most branches could never be loaded beyond their thermal limits, even under the most onerous generation and demand scenarios. Conversely, a small set of branches could generally be loaded to very high levels, consistent with the long-tailed nature of this phenomenon. An index of branch radiality was proposed to explore the effect of branch meshing, although results here were inconclusive. Future work may consider how a branch's reactance should be aligned with its thermal capacity to better mitigate congestion.

Acknowledgements

The author acknowledges the contributions of Dr. Priyanko Guha Thakurta, Dr. Alireza Soroudi and Prof. Andrew Keane at earlier stages of this manuscript, and the assistance of Ms. Charlotte Cuffe with the statistical distribution fitting.

References

[1] B. K. Sovacool, D. Nugent, and A. Gilbert, "Construction cost overruns and electricity infrastructure: An unavoidable risk?" *The Electricity Journal*, vol. 27, no. 4, pp. 112–120, 2014, ISSN: 1040-6190.

[2] B. K. Sovacool, A. Gilbert, and D. Nugent, "Risk, innovation, electricity infrastructure and construction cost overruns: Testing six hypotheses," *Energy*, vol. 74, pp. 906–917, 2014, ISSN: 0360-5442.

[3] H. Wan, J. D. McCalley, and V. Vittal, "Increasing thermal rating by risk analysis," *IEEE Transactions on Power Systems*, vol. 14, no. 3, pp. 815–828, 1999.

[4] M. H. Haque, "Determination of steady-state voltage stability limit using p-q curve," *IEEE Power Engineering Review*, vol. 22, no. 4, pp. 71–72, 2002. DOI: 10.1109/MPER.2002.4312118.

[5] R. Prada and L. J. Souza, "Voltage stability and thermal limit: Constraints on the maximum loading of electrical energy distribution feeders," *IEE Proceedings-Generation, Transmission and Distribution*, vol. 145, no. 5, pp. 573–577, 1998.

[6] A. Kumar, S. Srivastava, and S. Singh, "Congestion management in competitive power market: A bibliographical survey," *Electric Power Systems Research*, vol. 76, no. 1, pp. 153–164, 2005, ISSN: 0378-7796.

[7] F. Wu, F. Zheng, and F. Wen, "Transmission investment and expansion planning in a restructured electricity market," *Energy*, vol. 31, no. 6, pp. 954–966, 2006, Electricity Market Reform and Deregulation, ISSN: 0360-5442. DOI: https://doi.org/10.1016/j.energy.2005.03.001.

[8] O. B. Tor, A. N. Guven, and M. Shahidehpour, "Congestion-driven transmission planning considering the impact of generator expansion," *IEEE Transactions on Power Systems*, vol. 23, no. 2, pp. 781–789, 2008. DOI: 10.1109/TPWRS.2008.919248.

[9] E. B. Fisher, R. P. O'Neill, and M. C. Ferris, "Optimal transmission switching," *IEEE Transactions on Power Systems*, vol. 23, no. 3, pp. 1346–1355, 2008.

[10] M. Khanabadi, Y. Fu, and C. Liu, "Decentralized transmission line switching for congestion management of interconnected power systems," *IEEE Transactions on Power Systems*, vol. 33, no. 6, pp. 5902–5912, 2018.

[11] T. Jibiki, E. Sakakibara, and S. Iwamoto, "Line flow sensitivities of line reactances for congestion management," in *2007 IEEE Power Engineering Society General Meeting*, 2007, pp. 1–6. DOI: 10.1109/PES.2007.385928.

[12] D. M. Divan, W. E. Brumsickle, R. S. Schneider, B. Kranz, R. W. Gascoigne, D. T. Bradshaw, M. R. Ingram, and I. S. Grant, "A distributed static series compensator system for realizing active power flow control on existing power lines," *IEEE Transactions on Power Delivery*, vol. 22, no. 1, pp. 642–649, 2007.

[13] X. Zhang, C. Xu, D. Shi, Z. Wang, Q. Zhang, G. Liu, K. Tomsovic, and A. Dimitrovski, "Allocation of a variable series reactor considering ac constraints and contingencies," *CSEE Journal of Power and Energy Systems*, vol. 5, no. 1, pp. 63–72, 2019.

[14] A. A. P. da Silva and J. M. de Barros Bezerra, "A model for uprating transmission lines by using htls conductors," *IEEE Transactions on Power Delivery*, vol. 26, no. 4, pp. 2180–2188, 2011.

[15] P. Marannino, P. Bresesti, A. Garavaglia, F. Zanellini, and R. Vailati, "Assessing the transmission transfer capability sensitivity to power system parameters," in *14th PSCC*, 2002, pp. 1–7.

[16] J.-R. Riba, Santiago Bogarra, Á. Gómez-Pau, and M. Moreno-Eguilaz, "Uprating of transmission lines by means of htls conductors for a sustainable growth: Challenges, opportunities, and research needs," *Renewable and Sustainable Energy Reviews*, vol. 134, p. 110 334, 2020.

[17] G. Crognier, P. Tournebise, M. Ruiz, and P. Panciatici, "Grid operation-based outage maintenance planning," *Electric Power Systems Research*, vol. 190, p. 106 682, 2021, ISSN: 0378-7796. DOI: https://doi.org/10.1016/j.epsr.2020.106682. [Online]. Available: https://www.sciencedirect.com/science/article/pii/S0378779620304855.

[18] B. Stott, J. Jardim, and O. Alsac, "DC power flow revisited," *IEEE Transactions on Power Systems*, vol. 24, no. 3, pp. 1290–1300, Aug. 2009, ISSN: 1558-0679. DOI: 10.1109/TPWRS.2009.2021235.

[19] J. A. Momoh, R. Adapa, and M. E. El-Hawary, "A review of selected optimal power flow literature to 1993. i. nonlinear and quadratic programming approaches," *IEEE Transactions on Power Systems*, vol. 14, no. 1, pp. 96–104, Feb. 1999, ISSN: 1558-0679. DOI: 10.1109/59.744492.

[20] P. Cuffe, "Optimization and visualization tools for situational awareness in highly renewable power systems," in *2020 6th IEEE International Energy Conference (ENERGYCon)*, IEEE, 2020, pp. 930–933.

[21] L. L. Garver, P. R. V. Horne, and K. A. Wirgau, "Load supplying capability of generation-transmission networks," *IEEE Transactions on Power Apparatus and Systems*, vol. PAS-98, no. 3, pp. 957–962, May 1979.

[22] E. Chiodo, A. Losi, R. Mongelluzzo, and F. Rossi, "Capability chart for electrical power systems," in *IEE Proceedings C (Generation, Transmission and Distribution)*, IET, vol. 139, 1992, pp. 71–75.

[23] P. Cuffe, P. Smith, and A. Keane, "Capability chart for distributed reactive power resources," *IEEE Transactions on Power Systems*, vol. 29, no. 1, pp. 15–22, 2014.

[24] A. Dwivedi and X. Yu, "A maximum-flow-based complex network approach for power system vulnerability analysis," *IEEE Transactions on Industrial Informatics*, vol. 9, no. 1, pp. 81–88, Feb. 2013.

[25] L. C. Freeman, "A set of measures of centrality based on betweenness," *Sociometry*, vol. 40, no. 1, pp. 35–41, 1977.

[26] L. C. Freeman, S. P. Borgatti, and D. R. White, "Centrality in valued graphs: A measure of betweenness based on network flow," *Social networks*, vol. 13, no. 2, pp. 141–154, 1991.

[27] J. Fang, C. Su, Z. Chen, H. Sun, and P. Lund, "Power system structural vulnerability assessment based on an improved maximum flow approach," *IEEE Transactions on Smart Grid*, vol. 9, no. 2, pp. 777–785, 2018.

[28] A. Albarakati and M. Bikdash, "Vulnerabilities of power grid due to line failures based on power traffic centrality of the line graph," in *SoutheastCon 2018*, IEEE, 2018, pp. 1–7.

[29] R. Espejo, S. Lumbreras, A. Ramos, T. Huang, and E. Bompard, "An extended metric for the analysis of power-network vulnerability: The line electrical centrality," in *2019 IEEE Milan PowerTech*, IEEE, 2019, pp. 1–5.

[30] M. J. Newman, "A measure of betweenness centrality based on random walks," *Social Networks*, vol. 27, no. 1, pp. 39–54, 2005, ISSN: 0378-8733.

[31] P. Crucitti, V. Latora, and S. Porta, "Centrality measures in spatial networks of urban streets," *Physical Review E*, vol. 73, no. 3, Mar. 2006, ISSN: 1550-2376.

[32] E. Bompard, D. Wu, and F. Xue, "Structural vulnerability of power systems: A topological approach," *Electric Power Systems Research*, vol. 81, no. 7, pp. 1334–1340, 2011.

[33] P. Hines and S. Blumsack, "A centrality measure for electrical networks," in *Proceedings of the 41st Annual Hawaii International Conference on System Sciences (HICSS 2008)*, Jan. 2008, pp. 185–185. DOI: 10.1109/HICSS.2008.5.

[34] E. Zio and R. Piccinelli, "Randomized flow model and centrality measure for electrical power transmission network analysis," *Reliability Engineering & System Safety*, vol. 95, no. 4, pp. 379–385, 2010.

[35] K. Wang, B.-h. Zhang, Z. Zhang, X.-g. Yin, and B. Wang, "An electrical betweenness approach for vulnerability assessment of power grids considering the capacity of generators and load," *Physica A: Statistical Mechanics and its Applications*, vol. 390, no. 23, pp. 4692–4701, 2011, ISSN: 0378-4371. DOI: https://doi.org/10.1016/j.physa.2011.07.031.

[36] P. Cuffe, "A comparison of malicious interdiction strategies against electrical networks," *IEEE Journal on Emerging and Selected Topics in Circuits and Systems*, vol. 7, no. 2, pp. 205–217, Jun. 2017, ISSN: 2156-3365.

[37] T. Verma, W. Ellens, and R. E. Kooij, "Context-independent centrality measures underestimate the vulnerability of power grids," *International Journal of Critical Infrastructures 7*, vol. 11, no. 1, pp. 62–81, 2015.

[38] P. Cuffe and A. Keane, "Novel branch centrality measures for electrical power systems considering both load-serving and circulating currents," in *2020 6th IEEE International Energy Conference (ENERGYCon)*, IEEE, 2020, pp. 707–712.

[39] S. M. Abdelkader, D. J. Morrow, and A. J. Conejo, "Network usage determination using a transformer analogy," *IET Generation, Transmission Distribution*, vol. 8, no. 1, pp. 81–90, 2014.

[40] G. A. Orfanos, P. S. Georgilakis, and N. D. Hatziargyriou, "A more fair power flow based transmission cost allocation scheme considering maximum line loading for n-1 security," *IEEE Transactions on Power Systems*, vol. 28, no. 3, pp. 3344–3352, 2013.

[41] E. Cotilla-Sanchez, P. D. H. Hines, C. Barrows, and S. Blumsack, "Comparing the topological and electrical structure of the north american electric power infrastructure," *IEEE Systems Journal*, vol. 6, no. 4, pp. 616–626, 2012.

[42] P. Cuffe, "A comparison of malicious interdiction strategies against electrical networks," *IEEE Journal on Emerging and Selected Topics in Circuits and Systems*, vol. 7, no. 2, pp. 205–217, Jun. 2017, ISSN: 2156-3365. DOI: 10.1109/JETCAS.2017.2704879.

[43] P. Hines, E. Cotilla-Sanchez, and S. Blumsack, "Do topological models provide good information about electricity infrastructure vulnerability?" *Chaos: An Interdisciplinary Journal of Nonlinear Science*, vol. 20, no. 3, p. 033 122, 2010. DOI: 10.1063/1.3489887. eprint: https://doi.org/10.1063/1.3489887. [Online]. Available: https://doi.org/10.1063/1.3489887.

[44] G. A. Pagani and M. Aiello, "The power grid as a complex network: A survey," *Physica A: Statistical Mechanics and its Applications*, vol. 392, no. 11, pp. 2688–2700, 2013.

[45] H. R. Baghaee, M. Mirsalim, and G. B. Gharehpetian, "Power calculation using rbf neural networks to improve power sharing of hierarchical control scheme in multi-der microgrids," *IEEE Journal of Emerging and Selected Topics in Power Electronics*, vol. 4, no. 4, pp. 1217–1225, 2016. DOI: 10.1109/JESTPE.2016.2581762.

[46] F. Capitanescu, "Critical review of recent advances and further developments needed in ac optimal power flow," *Electric Power Systems Research*, vol. 136, pp. 57–68, 2016.

[47] F. Capitanescu, J. M. Ramos, P. Panciatici, D. Kirschen, A. M. Marcolini, L. Platbrood, and L. Wehenkel, "State-of-the-art, challenges, and future trends in security constrained optimal power flow," *Electric Power Systems Research*, vol. 81, no. 8, pp. 1731–1741, 2011.

[48] R. D. Christie, B. F. Wollenberg, and I. Wangensteen, "Transmission management in the deregulated environment," *Proceedings of the IEEE*, vol. 88, no. 2, pp. 170–195, Feb. 2000.

[49] M. Papagelis, "Refining social graph connectivity via shortcut edge addition," *ACM Trans. Knowl. Discov. Data*, vol. 10, no. 2, Oct. 2015, ISSN: 1556-4681. DOI: 10.1145/2757281.

[50] R. D. Zimmerman, C. E. Murillo-Sánchez, and R. J. Thomas, "MATPOWER: Steady-state operations, planning, and analysis tools for power systems research and education," *IEEE Transactions on Power Systems*, vol. 26, no. 1, pp. 12–19, Feb. 2011, ISSN: 1558-0679. DOI: 10.1109/TPWRS.2010.2051168.

[51] J. Lofberg, "YALMIP: A toolbox for modeling and optimization in MATLAB," in *2004 IEEE International Conference on Robotics and Automation*, Sep. 2004, pp. 284–289.

[52] L. Gurobi Optimization, *Gurobi optimizer reference manual*, 2020. [Online]. Available: http://www.gurobi.com.

[53] C. Coffrin, D. Gordon, and P. Scott, *NESTA, the NICTA energy system test case archive*, 2014. arXiv: 1411.0359 [cs.AI].

[54] J. Lin, F. Kahrl, and X. Liu, "A regional analysis of excess capacity in china's power systems," *Resources, Conservation and Recycling*, vol. 129, pp. 93–101, 2018.

[55] P. Cuffe, *Raw data and scripts from "Maximising branch power flows as a descriptive structural metric for electrical networks"*, Jul. 2020. DOI: 10.6084/m9.figshare.12656738.

[56] ——, "Assortativity anomalies in a large test system," *IEEE Transactions on Power Systems*, vol. 31, no. 5, pp. 4169–4170, 2015.

[57] P. Cuffe and A. Keane, "Visualizing the electrical structure of power systems," *IEEE Systems Journal*, vol. 11, no. 3, pp. 1810–1821, 2015.

[58] M. Sahraei-Ardakani and K. W. Hedman, "A fast lp approach for enhanced utilization of variable impedance based facts devices," *IEEE Transactions on Power Systems*, vol. 31, no. 3, pp. 2204–2213, 2015.